Polymer Testing 128 (2023) 108221

Contents lists available at ScienceDirect

Polymer Testing

journal homepage: www.elsevier.com/locate/polytest

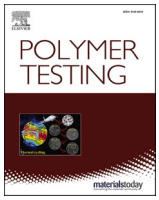

Effect of incorporating carbon- and silicon-based nanomaterials on the physico-chemical properties of a structural epoxy adhesive

Mohammad Al-Zu'bi [a], Lorna Anguilano [b,*], Mizi Fan [a]

[a] Department of Civil and Environmental Engineering, College of Engineering, Design and Physical Sciences, Brunel University London, UB8 3PH, United Kingdom
[b] Experimental Techniques Centre, College of Engineering, Design and Physical Sciences, Brunel University London, UB8 3PH, United Kingdom

ARTICLE INFO

Keywords:
Epoxy nanocomposites
Carbon- and silicon-based nanomaterials
Microstructural analysis
Chemical composition
Physical structure

ABSTRACT

Various carbon-based (i.e. carbon nanofibres (CNF), cellulose nanocrystals and graphite nanopowder) and silicon-based nanomaterials (i.e. silica nanopowder and MMT nanoclay) were incorporated into neat structural epoxy (NE) adhesive (Sikadur®-30) at 0.5, 1.0 and 1.5% by weight and mixed using a simple and cost-effective approach to produce the nanomaterial-modified epoxy adhesives (NMEAs). The impact of incorporating these nanomaterials into the NE on its chemical composition was investigated using Fourier transform infrared (FTIR) spectroscopy and Raman spectroscopy. X-ray diffraction (XRD) measurements were also used to identify the changes in the physical structure (i.e. the degree of crystallinity) that may occur in the NE with the addition of nanomaterials. Furthermore, the microstructure of the NE and NMEAs (in terms of the degree of dispersibility of the nanoparticles through the matrix) was investigated through scanning electron microscopy (SEM) analysis. A porosity analysis was also conducted across all samples. The results obtained from various tests were correlated to investigate the changes that occurred in the different properties of the matrix and the corresponding nanocomposites effectively and more critically. The SEM images showed some particle agglomeration, which increased with increasing wt%. An increase in the % porosity ratio of all nanocomposites over that of the NE was also observed, accompanied by a decrease in crystallinity compared to the NE. As per the FTIR spectroscopy, the chemical bonds in the NE and carbon-based NMEAs were observed to have different intensities, which were changed in the NMEAs, with the type and wt. % of the nanomaterials. No new bonds were formed by incorporating any of the nanomaterials (i.e. carbon- and silicon-based), except when adding 1.0 wt% CNF, where a bond at 1710 cm^{-1} was observed indicating a new C═O stretching bond. As shown by Raman spectroscopy, all CNF and graphite NMEAs exhibited higher I_D/I_G values than those of the corresponding pristine materials.

CRediT author statement

Mohammad Al-Zu'bi: Writing- Original draft preparation, Visualization. Lorna Anguilano: Writing- Reviewing and Editing. Mizi Fan: Investigation, Supervision.

1. Introduction

Owing to its high thermal and mechanical stabilities and superior chemical resistance and electrical isolating properties, in combination to its light weight, epoxy is considered one of the most important thermosetting polymers with a wide range of applications in the fields of, to name a few, adhesives, coatings, paints, innovative materials for the electronics and aerospace industries, electrical/electronic insulation and composite applications [1–4,49,51,52,84,99–101]. However, the highly cross-linked nature of epoxy resins results in inherently low fracture toughness and consequently poor resistance to fracture, which seriously restrict their applications. This leads to the need to improve the performance of epoxy resins [5].

Recently, introducing nano fillers into epoxy resins has received strong attention, due to their extraordinary thermo-mechanical and flame-retardant properties, which lead to obtain high strength, thermally stable and light weigh epoxy composites [5,102]. Among several nano fillers that can be used for preparing high performance epoxy nanocomposites, carbon nanomaterials, owing to their exceptional mechanical, thermal and physical properties, have become essential for the preparation of composites with multiple enhanced properties [5,45]. Those nanomaterials include carbon nanotubes (CNTs), graphene oxide

* Corresponding author.
E-mail address: lorna.anguilano@brunel.ac.uk (L. Anguilano).

https://doi.org/10.1016/j.polymertesting.2023.108221
Received 25 August 2023; Received in revised form 8 September 2023; Accepted 19 September 2023
Available online 21 September 2023

(GO), graphene nano platelets (GNP) and Nano sheets (GNS), graphite and carbon nanofibres (CNF).

Although CNTs are considered as one of the most effective nano fillers in the field of polymer composites and they could significantly improve both mechanical and thermal properties of epoxy adhesives, the high aspect ratio and flexibilities of CNTs along with the van der Waals forces between them cause CNTs to be severely entangled in close packing upon synthesis. Moreover, the chemically inert nature of CNTs leads to poor dispersibility and weak interfacial interactions with epoxy matrices. These issues would hinder the full utilisation of these particles in enhancing properties of epoxy adhesives [5]. Compared to CNTs, graphite platelets are about 500 times less expensive, and easily unfolded, whereas the CNT-based composites need an advanced processing technique in order to obtain uniform dispersion, waviness, and alignment of nanotubes [4]. CNFs, on the other hand, have a better chance in large-volume industrial applications than CNTs, due to their lower manufacturing cost (up to 500 times) and mass production scalability, and can be manufactured at high yields, which means that a lot of the reactant chemicals that were used successfully reacted to make the products, in addition to their good dispersion into epoxy resins. All those advantages have led to further in-depth investigation of their impact on epoxy nanocomposites [2,44,45].

It has been confirmed that incorporating carbon-based nanomaterials, such as CNTs [15,40,69,71–73,76–78,80,83,85–87], CNFs [6–10], graphene and graphite [17–23,69,70,74,82] and crystalline nano cellulose (CNC) [46–51] into epoxy resins improved their mechanical and thermal properties and were also found to provide outstanding reinforcing potential and demonstrates efficient stress transfer behaviour. Those improvements are attributed to the fact that incorporating the nanoparticles into epoxy provides strong interfacial interactions with the epoxy system through a chemical reaction, furthermore the uniform dispersion of the nanoparticles into epoxy enhances the bond between unreacted epoxy functional groups and nanoparticles, which eventually leads to arresting and suppressing the crack propagation, resulting ultimately in improved properties/performance [5].

In addition, silicon-based nanomaterials, such as silica [11–14,79,86] and clay [15,16,94] nanoparticles, have also showed their efficiency in improving both mechanical and thermal performance of epoxy polymers. For instance, Chisholm et al. [13] found that adding silicon carbide (SiC) to epoxy matrix led to enhanced mechanical properties. This improvement was credited to the uniform dispersion of the nanoparticles over the entire body of the matrix. Furthermore, the overall porosity of the composites was found to be reduced. It was also found that the thermal stability was improved by the addition of the nanoparticles, which was attributed to the additional cross-linking in the polymer owing to the catalytic effects produced by the presence of SiC nanoparticles. It was found by Hsour et al. [15] that adding montmorillonite (MMT) nanoclay into epoxy resin yielded an improvement in its mechanical properties. That was due to the uniform dispersion of nanoparticles, which ensured more viable sites for polymer and nanoparticles interaction, which also enhanced the thermal properties. Moreover, higher crosslinking between the nanoparticles and the epoxy molecules was observed, which eventually led to interlocking resin-nanoparticles structure in the matrix and might facilitate stress transfer process when the nanocomposite is loaded.

Introducing nanoparticles to polymer matrices has been also found to highly influence the chemical structure of the matrices. Hence, identifying the chemical reactions taking place and the changes happening in the chemical composition of the matrix as a result of introducing the nanoparticles is of high importance. Some effective tools have been adopted for those purposes, such as Fourier-transform infrared (FTIR) and Raman spectroscopies, which are used to better understand the molecular structure of materials through identifying the functional groups that appear and those that disappear because of the addition of the nanomaterials to the polymer, which eventually helps to know the characteristic changes that happen to the polymer.

Among the many studies [1–3,16,24–39,46,47,50,51,55–57,75,81] that have performed FTIR analysis on both pure epoxy matrices and the modified ones, only very few of them [16,26,33,75] have investigated the effect of adding nanoparticles on the chemical composition (i.e. changes in functional groups) of epoxy. For instance, Huttunen-Saarivirta et al. [16] concluded that the presence of the clay nanoparticles in the epoxy matrix did not show any new peaks, even though, the location of some of the characteristic IR peaks were shifted. Further investigation [26] found that when 0.5 wt% ultra-sonicated ozonolytic (USO) treated CNTs (OZ-CNTs) were dispersed in DGEBA epoxy resin, the formation of an esters peak corresponding to 1754 cm^{-1} was observed, which indicated that OZ-CNTs have reacted with the epoxy matrix. In another study done by Wang et al. [33], the FTIR analysis of epoxy specimens modified with CNT, GNP, and fullerene-C60 was investigated. It was found that the characteristic peaks for all specimens were identical, indicating that there was no new chemical bonding between the polymer and nano fillers. However, disappearance of the peak at a wavenumber of 913 cm^{-1} for all specimens indicated the ring-opening polymerization during crosslinking, which reflected the curing process. Montazeri [75] also observed no additional bands introduced when 2 wt% MWNT-OH was mixed with DGEBA epoxy.

Raman spectroscopy has also been considered in many studies [1–3,21,25,26,38,39,41–44,54,71] to investigate the chemistry of epoxy polymers and its nanocomposites. It's noteworthy that one of the most important characteristics of Raman analysis of carbon-based materials is the ratio of intensity of D/G bands (I_D/I_G), as it is a measure of the defects present on carbon nanomaterials structure. The G band is a result of in-plane vibrations of sp^2 bonded carbon atoms whereas the D band is due to out of plane vibrations attributed to the presence of structural defects. For example, it was observed in Ref. [1] that the Poly phosphamide (PPA)/epoxy and PPA-GNS/epoxy specimens exhibited the D band at 1358 cm^{-1} and the G band at 1593 cm^{-1}. Further investigation by Zhao et al. [3] indicated that almost no changes happened in the peak intensity ratios of disordered (D) band to G band of single-walled CNTs (SWCNTs) before (I_D/I_G = 0.09) and after adsorption of epoxy (i.e. EpPy-16) (I_D/I_G = 0.11). The typical Raman spectra of GNS-based epoxy resin in Ref. [42] exhibited the spectral ranges of D band at 1250–1450 and of G band at 1500~1700 cm^{-1}, which were ascribed to the location of the D and G peaks of the pure carbon-related materials (i.e. graphene), indicating the dispersion of the GNS in the epoxy matrix.

The degree of crystallinity of the polymer nanocomposite, which is a measure of the extent to which the material is crystalline, is also essential to be known and understood in order to predict the properties of the polymers and determine their potential fields of application. X-ray diffraction (XRD) [21,34,36–38,47,51,53,57,94] has widely been utilised for crystallinity determination.

Several studies investigated the effect of adding nanoparticles on the crystallinity of polymers [58–68]. For example, it was found that the nanoparticles in a polymer matrix can act as nucleating agents, which increase the crystallinity of the composite, or act as an impurity that hinders the formation of the ordered structure [58]. Mahmood et al. [59] found that the addition of amine functionalized CNTs to polyamide 6 (PA6) increased the crystallinity of the nanocomposites. Morimune et al. [60] studied GO-PVA (poly vinyl alcohol) nanocomposites, and it was found that the addition of GO led to increase the crystallinity of the nanocomposites from 28% for the neat PVA to 30%, 33%, 35% and 39% for 0.1%, 0.5%, 1%, and 5% GO loading, respectively. However, Bhattacharyya et al. [61] studied the graphene-reinforced ultrahigh molecular weight polyethylene (UHMWPE), and a reduction in crystallinity of the nanocomposites was observed. A study on PVA-cellulose nanocomposites was carried out by Kumar et al. [66], where a reduction in the crystallinity of the nanocomposite was observed. This was ascribed to the strong interaction of the CNCs with the –OH groups of PVA and twisting together into a confused mass between them, which eventually caused steric effect and destroyed the highly-ordered arrangement of

PVA.

Similar observations were reported by van Zyl et al. [62], where adding silica nanoparticles to PA6 was found to reduce its crystallinity and the crystallinity continued to decrease further with increase the silica concentration. Sadeghi et al. [63] also found that the crystallinity of the ethylene vinyl acetate (EVA)-silica nanocomposites dropped when compared to that of pure EVA. Similar results were reported by Chen et al. [64] in silica-PVA nanocomposites. On the other hand, another investigation on PVA-silica nanocomposites was carried out by Peng et al. [65]. It was found that there was an increase in the crystallinity of the PVA at a relatively low silica loading (i.e. 0.5 wt%), which was ascribed to the fact that the silica nanoparticles might be acting as a heterogeneous nucleating agent during crystallization.

Besides the techniques mentioned previously, scanning electron microscopy (SEM) analysis is also employed to examine the microstructure of the epoxy nanocomposites and to investigate the dispersibility of the nanoparticles through the matrix [1–3,16,21,26–29,33,34,37,38,41–44,48,75,88–96]. The porosity analysis of polymers has also been addressed but in few research studies [97,98].

As discussed so far regarding the chemical and physical characterisation of the epoxy nanocomposites, even though spectroscopic observations of the Nano-modified epoxy in terms of FTIR and Raman analyses were conducted in the literature, the chemical interaction of epoxy matrix with the nanoparticles is not fully present, hence, more in-depth understanding of the chemical changes within the epoxy nanocomposites is needed. Furthermore, most of the investigations that have addressed the crystallinity of the polymer nanocomposites were focusing on the thermoplastic polymers, while only few of them were interested in the thermosetting polymers (i.e. epoxy matrix), which also examined the effect of very few kinds of the nanoparticles that have an influence on the composites' crystallinity. Also, the porosity of the polymers and their accompanying nanocomposites has been scarcely studied and therefore, further research work is highly required. Investigating the porosity of the polymers and their corresponding nanocomposites has been scarce. Thus, there is a significant need for further research in this area.

This study undertakes a thorough investigation on the effect of incorporating carbon-based (i.e. CNF, cellulose nanocrystals and graphite nanopowder) and silicon-based (i.e. silica nanopowder and MMT nanoclay) nanomaterials into epoxy adhesive at three different concentrations, e.g. 0.5, 1.0 and 1.5% by weight of epoxy, on the microstructure, in terms of the nanoparticles dispersibility within the matrix and the porosity change, physical state and chemical composition of the matrix by means of SEM and porosity analyses, XRD measurements (i.e. crystallinity) and FTIR and Raman spectroscopies, respectively.

2. Materials and methodology

2.1. Materials

Epoxy adhesive: The Sikadur®-30, which was provided by Sika Limited, UK, was used. Sikadur®-30 is a thixotropic, structural 2-component adhesive, based on a combination of epoxy resins and special filler (A & B). The composition and the properties of the adhesive are shown in Tables 1 and 2, respectively.

Nanomaterials: Five types of nanoparticles (Fig. 1), which were provided by Nanografi, Turkey, were used for the purpose of this study, which are: CNF, silica nanopowder, cellulose nanocrystals (CNC), MMT nanoclay and graphite nanopowder. Their description and physical properties are listed in Table 2.

2.2. Methodology

2.2.1. Preparation of the neat epoxy and the nanocomposites

The neat epoxy (NE) samples were prepared by mixing the two components, part A (resin) and part B (hardener) (A: B = 3:1 by weight as recommended by the manufacturer) manually for 4 min.

For the NMEAs, some drops of acetone were first added to the nanoparticles and manually mixed for 3 min in order to improve the dispersibility of the nanoparticles and to reduce the agglomeration. Afterwards, the epoxy part A was carefully weighed and manually mixed for 2 min in a suitable beaker with the pre-weighted nanoparticles. The mix was then carried out through a high intensity ultrasonic irradiation for 5 min using Fisher Scientific FB 15051 with ultrasonic frequency of 37 kHz. Once the irradiation was completed, part B was then added to the modified part A and manually mixed for 2 min. After that, the whole mix of each sample was cast in a 1 cm-cubic rubber silicon mould and left to harden. A schematic that shows the procedure of the NMEAs production is illustrated in Fig. 2.

Table 1
Composition/ingredients of epoxy adhesive (As per supplier).

Part A		Part B	
Chemical name	Concentration (%)	Chemical name	Concentration (%)
Reaction product: bisphenol-A-(epichlorohydrin) (C15–H16–O2. C3–H5–Cl–O) x-) and epoxy resin (number average molecular weight ≤700)	≥10 - < 20	Quartz (SiO_2)	≥50 - ≤ 100
1,4-bis(2,3-epoxypropoxy) butane (C_{10}–H_{18}–O_4)	≥3 - < 5	2,2,4 (or 2,4,4)-trimethylhexane-1,6-diamine ($C_9H_{22}N_2$)	≥10 - < 20
Hydrocarbons, C10–C13, aromatics, <1% naphthalene	≥1 - < 2.5	Quartz, (SiO_2) <5 μm	≥0 - < 1

Table 2
Description and physical properties of nanomaterials (As per supplier).

Nanomaterial description (Purity)	Particle size	Density (g/cm^3)	Specific Surface Area (SSA) (m^2/g)
Carbon nanofibers (CNF) (>96%)	Outside Diameter: 190–590 nm, Length: 5.0–55.0 μm	2.2	20
Silicon Dioxide (SiO_2) nanopowder/nanoparticles, coated with 2 wt% Silane (97.3+ %)	16 nm (average)	2.2	150–550
Cellulose nanocrystals (nanocrystalline Cellulose, CNC) (92%)	Width: 10–20 nm, Length: 300–900 nm	1.49	~14
MMT nanoclay (99.9%)	800 nm	2.35 (Avg.)	Up to 450
Graphite (C) nanopowder/ nanoparticles (99.9%)	<50 nm	2.26	>100

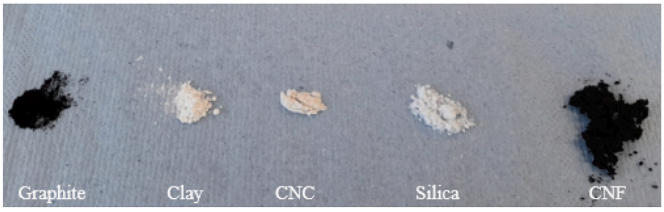

Fig. 1. Nanomaterials used in this study.

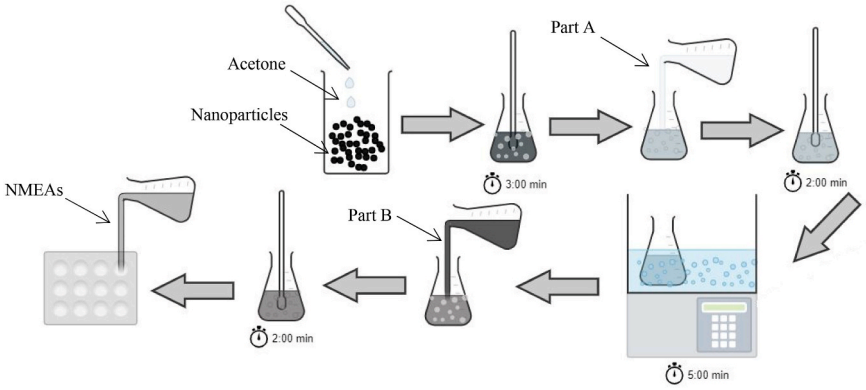

Fig. 2. Production of the NMEAs.

It is noteworthy that three different concentrations of the nanoparticles were considered in preparing the NMEAs samples, which are 0.5%, 1.0% and 1.5% by the total weight of epoxy (A + B). The designation of the NMEAs samples was the nanoparticles' name followed by the nanoparticles' concentration. For instance, the sample CNF-0.5 is the NMEA sample which is composed of epoxy adhesive loaded with 0.5 wt % of CNF.

2.2.2. Characterisation of the NE and the NMEAs

First, the SEM analysis was conducted on the samples using a Zeiss LEO and a Zeiss Supra 35VP microscopes. Moreover, the SEM images of samples' surfaces were also analysed through ImageJ software for the porosity study.

The crystallinity assessment was performed using a Bruker D8 Advance diffractometer equipped with copper tube and Lynxeye position sensitive detector. The diffractograms were recorded between a 2Theta range from 5° to 100°, with a scan step size of 1.0°, and then the crystallinity of each sample was obtained from the ration peak/backgrounds using the Bruker EVA software. The SEM analysis was conducted using a Zeiss LEO and a Zeiss Supra V35.

The investigation of the functional groups of both the NE and the NMEAs samples was performed by means of FTIR spectroscopy PerkinElmer Spectrum One, considering the wavenumber range from 4000 to 600 cm^{-1} at a resolution of 4 cm^{-1}. FTIR study of the nanoparticles was carried out with KBr pellets technique. The KBr pellets were prepared by mixing the nanoparticles with KBr powder (around 1:100) and using a hydraulic press at the pressure of 10 tonnes. The Raman spectroscopy was conducted using RENISHAW inVia Raman Microscope, considering the Raman shift range from 0 to 3200 cm^{-1} to test the NE and the NMEAs samples, and from 1000 to 3200 cm^{-1} to test the pristine nanomaterials. The spectra were collected by accumulating 5 scans.

3. Results and discussion

3.1. SEM and porosity analyses

The NMEAs samples were analysed by SEM to investigate their microstructure and morphology in terms of the degree of dispersibility of the nanoparticles through epoxy matrix, that is, whether they are agglomerating or uniformly dispersed through the matrix. Moreover, the % porosity of the NE and the nanocomposites in terms of the amount of the air voids appearing on their surfaces was also considered. The NE sample was also analysed in order to assess the distribution of the quartz grains prior the addition of the nanoparticles to benchmark the nano-modified materials against it. High-magnification SEM images of the NE and the NMEAs are shown in Fig. 3. The SEM images of the samples' surfaces are shown in Fig. 4, and the % porosity of samples is provided in Table 3.

3.1.1. SEM analysis

As shown in Fig. 3, as the nanoparticles' wt% within the matrix increases, a noteworthy phenomenon comes to light — the progressive agglomeration of nanoparticles. This agglomeration, the clumping together of nanoparticles, becomes more pronounced at higher concentrations due to the enhanced likelihood of nanoparticle collisions and interactions. As nanoparticles draw closer in proximity, attractive forces, such as van der Waals interactions (more in the carbon-based materials), can lead to their aggregation, forming larger clusters. Moreover, as the concentration increases, there's a higher likelihood of nanoparticle agglomeration due to the increased number of nanoparticles trying to occupy the same space.

This agglomeration has far-reaching consequences on the materials' (i.e. nanocomposites) structural integrity and porosity, as discussed in detail in the next section. The clustered nanoparticles introduce localized regions of increased particle density, altering the distribution of void spaces. These regions of heightened nanoparticle concentration can disrupt the uniformity of polymer chain interlocking during curing, rendering certain areas more susceptible to void formation. Consequently, the increase in nanoparticle agglomeration with rising concentrations serves as a crucial factor in shaping the observed linear relationship between concentration and % porosity. The intricate interplay between aggregation dynamics, curing kinetics, and polymer mobility underscores the multifaceted nature of nanoparticle-polymer interactions and their intricate impact on material porosity profiles.

3.1.2. Porosity analysis

First, it's worthy to note that porosity refers to the presence of empty spaces (i.e. air voids) within a material. In this study, % porosity in terms of the samples' surface area were considered, which typically refers to the percentage of the air voids present on the external surface of a sample relative to its total surface area. It's noteworthy that the previous definition of the porosity may appear unconventional, however, it has been chosen to emphasize the examination of voids specifically on the external surface, aligning with our research focus on surface properties and adhesion.

In this section, a detailed assessment of porosity within the nanocomposite systems is conducted, examining the % porosity increases in comparison to the NE for both carbon-based and silicon-based nanocomposites. Additionally, comprehensive performance comparisons are provided between the two nanocomposite families and within each family is provided and the influence of nanoparticle modifications on porosity was quantified, as presented in Table 3, while offering further insights to enhance understanding of porosity changes within these materials.

3.1.2.1. Comparison between NE and NMEAs. It was observed that the NE had lower porosity than those of the NMEAs. The shorter mixing time

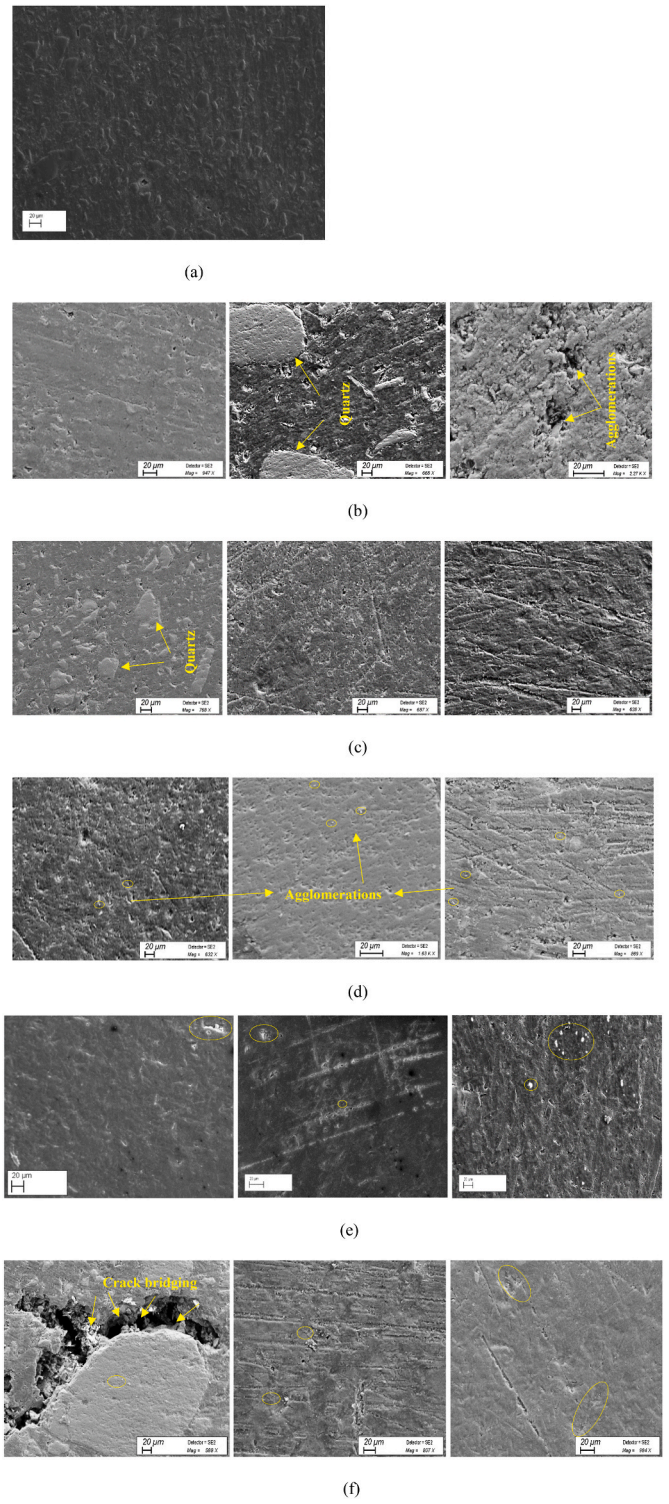

Fig. 3. SEM images of (a) NE, (b) CNF-0.5. CNF-1.0 and CNF-1.5 (from left to right), (c) Silica-0.5, Silica-1.0 and Silica-1.5, (d) Cellulose-0.5, Cellulose-1.0 and Cellulose-1.5, (e) Clay-0.5, Clay-1.0 and Clay-1.5 and (f) Graphite-0.5, Graphite-1.0 and Graphite-1.5.

of the NE could be amongst the reasons behind "catching" less amount of air voids (i.e. less % porosity) than in the case of the NMEAs.

For the NMEAs, as shown in Fig. 3 and Table 4, air bubbles showed up on the surface of all samples, but unevenly, where more air bubbles showed in some samples than others. This difference was attributed to differences in the curing conditions, specifically, curing time, where the % porosity is inversely proportional to curing time. Longer curing times allow more air bubbles to escape, resulting in less porosity. In other words, if a polymer is not fully cured within a specified time, it might retain some degree of mobility among its polymer chains. This mobility could allow trapped air or volatiles to escape during the curing process, leading to reduced porosity. As the curing time increases, the polymer chains become more crosslinked, reducing the potential for trapped voids, and vice versa.

Furthermore, the integration of diverse nanomaterials into epoxy polymer matrices introduces a sophisticated interplay of factors that intricately shape material porosity. Each nanomaterial type, distinguished by its SSA, density and wt% concentration, contributes distinctly to the observed variations in porosity, underlining the intricacies of nanoparticle-polymer interactions.

Nanomaterials characterized by higher SSA, such as graphite and silica nanopowders, offer an abundance of reactive sites, engendering nucleation sites for void generation during curing. This characteristic inclination is palpably reflected in the observed increase in porosity with ascending concentration levels. Conversely, nanomaterials with a relatively lower SSA, such as cellulose nanocrystals and CNF, exhibit a nuanced interplay of effects encompassing aggregation and concentration. While limited nucleation sites are intrinsic due to their lower SSA, the emergence of concentration-driven aggregation and the consequential modifications in curing kinetics potentially account for the observed fluctuations in porosity.

The distinctive SSA of nanoclay begets an intricate correlation between porosity and concentration, marked by an intriguing increase in porosity with elevated concentrations. While its higher SSA initially suggests an ample platform for nucleation, the observed rise in porosity at higher concentrations reveals a complex interplay of factors that override the straightforward association between SSA and porosity. This phenomenon of increased porosity challenges the conventional expectation of porosity reduction with higher SSA and demonstrates the dominance of concentration-dependent influences. These may encompass aggregation dynamics, intricate mechanistic nuances, and interactions with the polymer matrix. Similarly, graphite nanopowder, exhibiting a relatively moderate SSA, showcases nuanced behaviour with fluctuations in porosity at varying concentrations. These thought-provoking observations collectively underscore the multifaceted nature of nanoparticle-polymer interactions, where factors beyond SSA, including concentration-dependent effects, wield substantial influence over the material's porosity profile.

The intriguing relationship between nanoparticle concentration and porosity manifests as a complex interplay of diverse mechanisms. As the concentration of nanoparticles within the epoxy polymer matrix increases, several contributing factors converge to promote heightened % porosity. Firstly, an elevated nanoparticle concentration fosters a denser nanoparticle packing, thereby leading to increased obstacles for polymer chain mobility during curing. This phenomenon impedes the creation of an ideal, tightly knit network structure and paves the way for the formation of voids. These voids result from the inability of the polymer chains to uniformly interlock due to the presence of closely spaced nanoparticles. Consequently, the aggregation of nanoparticles amplifies the likelihood of forming regions of low-density material, culminating in the observed higher porosity.

Furthermore, the augmented concentration of nanoparticles engenders a greater concentration of potential nucleation sites for void formation. These nucleation sites originate from the nanoparticles' surfaces, which offer reactive sites for the initiation of voids during the curing process. As the nanoparticle concentration increases, the density of these initiation points surges, facilitating the generation of voids upon curing. This interaction is accentuated by nanoparticles with higher SSA's, such as graphite and silica nanopowder, which provide a surplus of active sites for nucleation. Consequently, the combined influence of hindered polymer chain mobility and a heightened density of nucleation sites synergistically fosters an environment conducive to greater

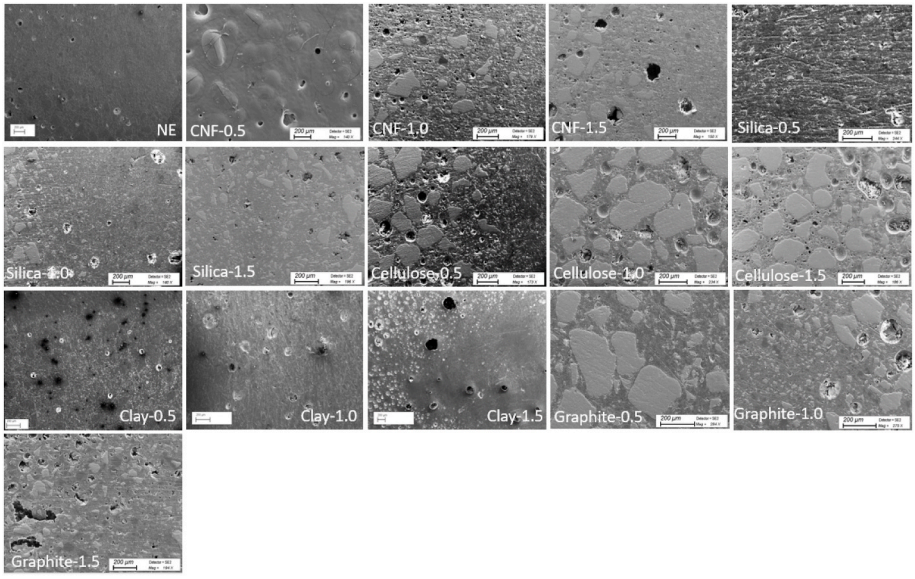

Fig. 4. SEM images of surfaces of the NE and the NMEAs samples.

Table 3
% Porosity of the NE and the NMEAs.

Nanocomposite	Sample	% Porosity	% Porosity increase of the NMEAs compared to the NE	% Porosity increase of the NMEAs with the wt % increase	
				From 0.5 to 1.0 wt %	From 1.0 to 1.5 wt %
	NE	2.015	–		–
CNF	CNF-0.5	2.501	24.1	7.0	4.6
	CNF-1.0	2.676	32.8		
	CNF-1.5	2.800	39.0		
Silica	Silica-0.5	2.630	30.5	2.9	2.7
	Silica-1.0	2.734	35.7		
	Silica-1.5	2.807	39.3		
Cellulose	Cellulose-0.5	2.945	46.2	11.8	8.5
	Cellulose-1.0	3.292	63.4		
	Cellulose-1.5	3.571	77.2		
Clay	Clay-0.5	2.225	10.4	21.2	15.0
	Clay-1.0	2.697	33.8		
	Clay-1.5	3.101	53.9		
Graphite	Graphite-0.5	2.395	18.9	12.4	6.1
	Graphite-1.0	2.693	33.6		
	Graphite-1.5	2.856	41.7		

Table 4
% Crystallinity of the NE and the NMEAs.

Sample	% Crystallinity	% Crystallinity decrease of the NMEAs compared to the NE
NE	65	–
CNF-0.5	43.8	32.6
CNF-1.0	42.5	34.6
CNF-1.5	41.5	36.2
Silica-0.5	50.4	22.5
Silica-1.0	48.0	26.2
Silica-1.5	47.0	27.7
Cellulose-0.5	52.1	19.8
Cellulose-1.0	48.9	24.8
Cellulose-1.5	46.7	28.2
Clay-0.5	54.9	15.5
Clay-1.0	51.2	21.2
Clay-1.5	48.9	24.8
Graphite-0.5	54.7	15.8
Graphite-1.0	49.3	24.2
Graphite-1.5	45.7	29.7

porosity.

Moreover, it was observed, as shown in Tables 3 and it is evident that the increase in the NMEAs porosity is more pronounced when moving from 0.5 to 1.0 wt% concentrations (i.e. 100% concentration increase) than in the case of 50% further increase in the concentration (i.e. from 1.0 to 1.5 wt%). This was attributed to that, since the particles agglomerations and clustering increase with the concentration, when nanoparticles cluster together, forming groups or agglomerations, they tend to occupy certain areas within the material more densely compared to other regions. These dense regions with a higher concentration of nanoparticles are what we refer to as "regions of concentrated

nanoparticles". Now, these agglomerations of nanoparticles don't fit perfectly within the material's structure, and they can create irregularities or gaps between them and the surrounding matrix.

Therefore, these two effects — the concentration of nanoparticles in certain areas and the formation of voids due to agglomeration — work together to influence the overall structure of the material. When there are areas with concentrated nanoparticles and voids, the material's overall arrangement becomes less uniform. This lack of uniformity disrupts the optimal arrangement of polymer chains and nanoparticles that is necessary for minimizing porosity.

In summary, the specific attributes of each nanoparticle type, including the SSA and density, synergistically interact with their concentration to exert a profound influence on the observed % porosity in NMEA samples. The linear correlation between concentration and porosity highlights the essential role of considering a comprehensive array of factors that extend beyond concentration alone. Among these pivotal factors are nanoparticle behaviour, intricate interactions, and the intricacies of curing kinetics. The harmonious interplay of these elements serves to precisely delineate the distinctive contribution of each nanoparticle type and its concentration to the overall porosity observed within the NMEA samples.

3.1.2.2. Comparison between the different NMEAs. First, in the context of the carbon-based nanocomposites — CNF, cellulose and graphite — a non-consistent trend in porosity changes, with the wt%, compared to the NE was observed. As the nanoparticle concentration increased from 0.5 to 1.0 wt%, the order of % porosity increases consistently followed "CNF < cellulose < graphite". However, when the concentration is further elevated from 1.0 to 1.5 wt%, the order shifted to "CNF < graphite < cellulose", as shown in Table 3.

The observed variations in % porosity increases among the nanocomposites stem from a multifaceted interplay of critical factors. These include the distinctive attributes of nanoparticle size, shape, SSA, agglomeration behaviour, and concentration effects, which collectively influence their performance within the epoxy matrix.

Nanoparticle size plays a pivotal role in determining their efficacy in reducing porosity. CNF, despite exhibiting a wide size range, possesses a notable length advantage, which allows it to effectively bridge and fill voids within the epoxy matrix. On the other hand, cellulose, with its smaller width and shorter length, offers a lower SSA (~14 m^2/g) but may compensate through increased opportunities for interaction with the epoxy, potentially leading to superior dispersion and porosity reduction. Meanwhile, graphite nanoparticles, with their diminutive size, may face challenges related to agglomeration, impeding their ability to uniformly fill voids and reducing their overall effectiveness in porosity reduction.

Interestingly, the changing order of % porosity increase from 0.5 to 1.0 wt% and 1.0 to 1.5 wt% concentrations suggests a nuanced relationship between nanoparticle concentration and porosity reduction. At lower concentrations (0.5–1.0 wt%), CNF, with its remarkable aspect ratio and length, might dominate in porosity reduction. However, as the concentration increases further (1.0–1.5 wt%), the smaller graphite particles may become more effective, potentially overcoming their initial limitations. This phenomenon underscores the importance of considering concentration-dependent saturation effects in nanocomposite design.

Furthermore, the unique characteristics inherent to each nanoparticle type significantly impact their performance within the epoxy matrix. Variability in factors such as dispersion, distribution, and chemical interactions introduces sample-to-sample differences, which can influence the observed results.

Second, in the realm of silicon-based nanocomposites, encompassing silica and clay nanoparticles, a persistent order of % porosity increase (clay ≫ silica) when compared to the NE comes to the forefront. This order remains consistent across varying wt% concentrations, notably from 0.5 to 1.0 wt% and from 1.0 to 1.5 wt%.

These observations can be explained by examining the distinct material properties of clay and silica and considering several key factors. For instance, the SSA of the silicon-based nanoparticles emerging as a pivotal element. Silica nanoparticles, boasting an SSA ranging from 150 to 550 m^2/g, and clay particles, with a maximum SSA of 450 m^2/g, showcase differences in their potential for interaction with the epoxy matrix. The higher SSA of silica grants it an augmented number of interaction sites with the epoxy, enabling superior dispersion and enhanced porosity reduction. In contrast, although clay nanoparticles exhibit a respectable SSA, their larger size may limit their effectiveness in uniformly filling voids and reducing porosity.

Nanoparticle size remains a critical determinant in shaping their performance within the epoxy matrix. Silica, characterized by an average size of 16 nm, significantly outpaces clay, which has a larger average size of 800 nm. This substantial size difference underscores silica's adeptness at penetrating and effectively filling gaps within the epoxy matrix, resulting in a pronounced reduction in porosity.

Agglomeration tendencies further influence porosity reduction. Smaller silica nanoparticles exhibit a lower propensity for agglomeration, ensuring a more uniform dispersion within the epoxy matrix. Conversely, clay nanoparticles, due to their larger size, may encounter more pronounced agglomeration, compromising their ability to uniformly fill voids and thus reducing their overall effectiveness in porosity reduction.

The unwavering order of % porosity increase across different concentration ranges signifies the robustness of this phenomenon. This consistency underscores the need to consider concentration-independent factors, such as particle size, SSA, and agglomeration behaviour, as the primary drivers behind the observed trend.

Finally, in comparing the carbon-based and silicon-based nanocomposites, a notable difference emerges in their porosity changes relative to the NE. The carbon-based nanocomposites exhibited a varying order of % porosity increase with changing concentrations. In contrast, the silicon-based nanocomposites consistently maintained the order of % porosity increase across different concentration increases. This distinction underscores the complexity and variability inherent in carbon-based nanocomposite systems, while the silicon-based counterparts demonstrated a more consistent and predictable behaviour in % porosity increase.

Therefore, to gain a more comprehensive understanding of these intricate interactions and further optimize nanocomposite materials, additional experimental studies and computational modelling efforts are warranted. These endeavours will enable a deeper exploration of the dynamic relationships between nanoparticle properties, concentration, and their effects on porosity reduction, ultimately contributing to the refinement of nanocomposite design and engineering.

3.2. Crystallinity analysis

The % crystallinity of the NE and the NMEAs samples is provided in Table 4. It was observed that all NMEAs, regardless of the nanomaterial type or their wt%, had lower % crystallinity than that of the NE.

For the CNF nanocomposites, the crystallinity reduction, which disagrees with what was found by Mahmood et al. [59], can be attributed to the influence of CNF on the behaviour of the epoxy matrix. Specifically, the presence of CNF can create a physical barrier that hampers the movement of epoxy chains, thereby diminishing their capacity to organize themselves into well-structured arrangements. Consequently, the polymer chains encounter limitations in their ability to achieve the necessary regular alignment for the development of crystalline domains. Furthermore, the process of crystallization hinges on the availability of specific sites where crystals can initiate and grow. The incorporation of CNF can, in some instances, disrupt the formation of these critical nucleation sites or even impede their development, ultimately leading to a reduction in the overall crystallinity of the

material. While for the cellulose nanocomposites, the crystallinity reduction was ascribed to the strong interaction of the cellulose with the OH groups of the epoxy forming a twisted mass, causing steric effect, which resulted in the destruction of the epoxy-ordered structure, as confirmed by Kumar et al. [66]. Whereas in the case of incorporating the graphite nanoparticles, the crystallinity reduction is ascribed to, as reported by Bhattacharyya et al. [61], that the exfoliated state of graphite, which restricted the free movement of polymer chains to arrange themselves in an orderly fashion, hindering the crystallization, thus reducing its crystallinity.

For the silicon-based nanocomposites, the crystallinity decrease below that of the NE could be, as observed in Refs. [62,63], due to the fact that adding silica nanoparticles to the polymer decreased the chain orders which in turn disturbed the crystallization process, which can be an indication of the reduction in crystalline areas of epoxy. Similar interpretation could be drawn in the case of adding clay nanoparticles.

It was also found that the % crystallinity of the NMEAs decreased with the wt%. This can be due to both nanoparticle agglomerations and increased porosity with the wt%, which would introduce structural complexities that hinder the establishment of ordered molecular arrangements. These factors contribute to reduced crystallinity by preventing the formation of well-defined and organized crystalline regions within the material.

More specifically, when nanoparticles agglomerate, they create zones of constrained molecular movement, impeding the polymer chains' ability to achieve the necessary alignment for crystalline structures. Furthermore, these agglomerations disrupt the formation of nucleation sites, which are pivotal for initiating the growth of well-defined crystalline regions. The irregularities introduced by these agglomerations hinder the material's capacity to achieve the desired ordered arrangement, resulting in reduced crystallinity. Furthermore, agglomerations or uneven distribution of nanoparticles can create areas of differing polymer density, leading to variations in crystallinity. The interface between the nanoparticles and the epoxy matrix can introduce irregularities in the molecular arrangement. These irregularities can propagate throughout the material, affecting the overall crystalline structure. The stress and strain at the interface can also influence crystallization behaviour.

The influence of increased porosity on reduced crystallinity in materials is rooted in the intricate interplay between molecular arrangement, density, and nucleation sites. Porosity refers to the presence of voids or open spaces within a material's structure, which can arise from incomplete packing of molecules or the inclusion of gas or other substances. This porosity introduces a level of complexity that significantly impacts the material's ability to form and maintain well-defined crystalline regions.

One of the primary mechanisms by which increased porosity contributes to reduced crystallinity is through the disruption of molecular packing. In a crystalline material, polymer chains ideally arrange themselves in an organized and tightly packed manner. However, the presence of voids and gaps hinders the optimal arrangement of these chains, preventing them from achieving the required alignment for crystalline growth. As a result, the material experiences decreased crystallinity because the irregular void-filled regions prevent the propagation of ordered structures.

Furthermore, the presence of porosity limits the availability of suitable nucleation sites. Nucleation sites are specific locations within a material where the initiation of crystalline growth occurs. In porous materials, the irregular surfaces of voids and pores do not possess the necessary characteristics for effective nucleation. This deficiency in proper nucleation sites disrupts the crystallization process, as the growth of crystals necessitates organized starting points. Without adequate nucleation sites, the material's ability to develop well-structured crystalline regions becomes compromised.

In essence, increased porosity acts as a barrier to both molecular alignment and nucleation site availability, culminating in a reduction of crystallinity. The irregularities introduced by the presence of voids and gaps prevent the formation of the orderly arrangements essential for crystalline growth. As a result, materials with heightened porosity exhibit diminished crystallinity due to the challenges posed to the establishment of well-defined, organized molecular structures.

It's noteworthy that, consistent with what was revealed in the case of porosity change with the concentration, the crystallinity of the nanocomposites showed higher decrease when doubling the concentration (i.e. from 0.5 to 1.0 wt%) compared to when the concentration was further increased by an additional 50%. This was due to, as discussed previously, the relationship between porosity and crystallinity.

3.3. FTIR spectroscopy

FTIR analysis was performed to assess the intensities of functional groups in both the NE and the carbon-based NMEAs. The study examines the intensity orders of various functional groups and their corresponding wavenumbers. The comparison helps assess the chemical changes brought about by the incorporation of nanoparticles to the epoxy resin. The order of intensities is used to evaluate changes in the composition. The analysis is presented for the carbon-based NMEAs. New peaks and disappearing peaks in the NMEAs compared to the nanoparticles and epoxy are also discussed. Changes in functional groups and their appearance or disappearance indicate interactions between the nanoparticles and the epoxy matrix. This section provides detailed information on intensity changes, wavenumbers, and specific functional groups affected in each nanocomposite.

The intensity order of the functional groups and their corresponding wavenumbers that showed in NE and the carbon-based NMEAs samples is listed in Table 5 and it is used as a base to assess the chemical changes. Also, Fig. 5 shows the FTIR spectrum of those samples. It's noteworthy that the numbers 0.5, 1.0 and 1.5 in Table 5 indicate the carbon-based NMEAs samples with 0.5, 1.0 and 1.5 wt% concentration of nanoparticles, respectively. Moreover, the intensity order, for instance, NE < 0.5 < 1.0 <1.5 indicates that the intensity of a bond is the minimum in the NE sample, higher in the samples prepared with 0.5 wt% followed by that made with 1.0 wt% sample and the highest in the 1.5 wt% one.

As shown in Table 5 and Fig. 5, the intensity of the N–H bending vibration in all nanocomposite was higher than in the NE sample. Moreover, it was observed that it increased with the wt% of the nanoparticles. Similarly, C–C stretching was also found to have the same behaviour in the CNF and cellulose samples at 1605.7 cm^{-1}, and in graphite sample at 1581 cm^{-1}. The $–CH_2$- (acyclic)/CH stretching, which corresponds to 2921.8 and 2851 cm^{-1} and the asym. $–CH_2$ deformation at 1295.8 cm^{-1} also show the same trend in the CNF samples. Moreover, the same observation was found for the C–C stretching at 1581 cm^{-1} and the asym. aromatic C–O stretch at 1237.6 cm^{-1}, but the former (i.e. C–C stretching at 1581 cm^{-1}) disappeared in the samples CNF-1.0 and CNF-1.5, which also did not have the latter functional group. The same order was also noticed in the cellulose samples for the functional groups acyclic diaryl ethers, =C–O–C = at 1180.3 cm^{-1}, C–O–C str./C–H bonds at 1077.2 cm^{-1} and = C–O–C (sym. C–O str.) at 1032.2 cm^{-1}, which also followed the same order in the graphite sample, but at 1035.8 cm^{-1}.

On the other hand, it was observed that the intensity orders in some of the nanocomposites are not proportional to the wt% concentration of the nanomaterials. For example, in the cellulose samples the intensity order (i.e. NE < 0.5 < 1.5<1.0) showed for the C–C stretching at 1582 cm^{-1}, and in the graphite samples for the $–CH_2$- (acyclic)/CH stretching at 2921.8 and 2851.8 cm^{-1} and the C–C stretching at 1605.7 cm^{-1}.

Other intensity orders were observed to show in only one nanocomposite. For example, the order NE < 1.0 < 0.5<1.5 and the order NE < 1.5 < 0.5<1.0 appeared in the functional groups CH_3 sym. bending vib/asym. CH_3 def. vib at 1413.1 cm^{-1} and in the = C–O–C (sym. C–O str.) at 1028.6 cm^{-1}, respectively.

In cellulose samples, the intensity order 1.0 < 1.5<0.5 < NE was

Table 5
The intensity order of the functional groups that showed in the NE and the carbon-based NMEAs.

NMEAs	Wavenumber (cm^{-1})	Functional group(s)	The intensity order (lower to higher)
CNF			
	3318	N–H bending vibration/ N–H stretching	NE < 0.5 < 1.0<1.5
	2921.8	CH stretching	NE < 0.5 < 1.0<1.5
	2851	CH stretching	NE < 0.5 < 1.0<1.5
	1605.7	C═C stretching	NE < 0.5 < 1.0<1.5
	1581	C–C stretching	NE < 0.5 < 1.0<1.5
	1413.1	CH_3 sym. bending vib/ asym CH_3 def. vib	NE < 1.0 < 0.5<1.5
	1295.8	asym –CH_2 deformation	NE < 0.5 < 1.0<1.5
	1237.6	asym aromatic C–O stretch	NE < 0.5 < 1.0<1.5
	1028.6	= C–O–C (sym. C–O str.)	NE < 1.5 < 0.5<1.0
Cellulose			
	3318	N–H bending vibration/ N–H stretching	NE < 0.5 < 1.0<1.5
	2921.8	CH stretching	1.0 < NE < 0.5 < 1.5
	2851.8	CH stretching	1.0 < NE < 0.5 < 1.5
	2502	-OH str./O–H str.	1.0 < 1.5<0.5 < NE
	1605.7	C═C stretching	NE < 0.5 < 1.0<1.5
	1582	C–C stretching	NE < 0.5 < 1.5<1.0
	1413.1	CH_3 sym. bending vib/ asym. CH_3 def. vib	1.0 < 1.5<0.5 < NE
	1295.6	asym –CH_2 deformation	1.5 < 1.0<0.5 < NE
	1237	asym aromatic C–O stretch	1.0 < 0.5 < NE < 1.5
	1180.3	acyclic diaryl ethers, =C–O–C =	NE < 0.5 < 1.0<1.5
	1077.2	C–O–C str./C–H bonds	NE < 0.5 < 1.0<1.5
	1032.2	= C–O–C (sym. C–O str.)	NE < 0.5 < 1.0<1.5
Graphite			
	3305.7	O–H str	NE < 0.5 < 1.0<1.5
	2921.8	Asym. C–H stretching	NE < 0.5 < 1.5<1.0
	2851.8	Sym. C–H stretching	NE < 0.5 < 1.5<1.0
	1605.7	C═C stretching	NE < 0.5 < 1.5<1.0
	1581	C–C stretching	NE < 0.5 < 1.0<1.5
	1429.5	CH_2 del' vib/sym. CO_2 – str./asym. CH_3 def. vib	1.5 < NE < 0.5 < 1.0
	1298.4	asym –CH_2 deformation	1.5 < NE < 0.5 < 1.0
	1241	C–OH str	1.5 < 0.5 < NE < 1.0
	1179.8	acyclic diaryl ethers, =C–O–C =	1.0 < NE < 0.5 < 1.5
	1081.3	C–O–C str.	1.0 < NE < 0.5 < 1.5
	1035.8	= C–O–C (sym. C–O str.)	NE < 0.5 < 1.0<1.5

found to be followed for the functional groups –OH str./O–H str. at 2502 cm^{-1} and for the CH_3 sym. bending vib/asym. CH_3 def. vib at 1413.1 cm^{-1}. While the functional group –CH_2- (acyclic)/CH stretching at 2921.8 and 2851.8 cm^{-1} was found to follow the order 1.0 < NE < 0.5 < 1.5. and finally, the groups asym. -Ch_2 deformation at 1295.6 cm^{-1} and asym. aromatic C–O stretch at 1237 cm^{-1} were found in the order 1.5 < 1.0<0.5 < NE and 1.0 < 0.5 < NE < 1.5, respectively.

The order 1.5 < NE < 0.5 < 1.0 showed, in the graphite samples, was followed by the CH_2 del' vib/sym. CO_2 – str./asym. CH_3 def. vib at 1429.5 cm^{-1} and the asym. –CH_2 deformation at 1298.4 cm^{-1}. In the same samples, the functional groups acyclic diaryl ethers, =C–O–C = at 1179.8 cm^{-1} and C–O–C str./C–H bonds at 1081.3 cm^{-1} followed the intensity order 1.0 < NE < 0.5 < 1.5.

In addition to the changes shown in the intensity of some chemical bonds, further changes in the chemical composition of the raw materials, e.g. epoxy matrix and the pristine nanomaterials, were observed. Where new functional groups appeared in the NMEAs, that were not there in the raw materials, and others disappeared from the raw materials as a result of the interaction between the nanoparticles and the epoxy matrix.

It was observed that all the carbon-based NMEAs showed disappearance of the C═C bond, which appeared at about 1632 cm^{-1}, 1639 cm^{-1} and 1632 cm^{-1}, in the spectrum of the nanoparticles, respectively, which was also observed in Refs. [37,38] for GO nanoparticles at 1631 cm^{-1}, and its presence was also confirmed in cellulose nanofibres at 1640 cm^{-1} [51]. Furthermore, it was observed that CNF-1.5 showed disappearance of the NH_2 group/aromatic C═C str. at 1508 cm^{-1}, which was confirmed that they are there in epoxy at that wavenumber [15,50].

For cellulose nanocomposites, the O–H stretching vibration of the OH groups at about 3417 cm^{-1} and C–H stretching vibration at about 2901 cm^{-1}, which where there in the nanoparticles, which were also noticed in Ref. [50] between 3500 and 3000 cm^{-1} and 2901 cm^{-1}, respectively, disappeared in all the cellulose NMEAs samples. Moreover, in agreement with [46,50], bands at 1112, 1059 and 898 cm^{-1}, assigned to C–O stretching and the glycosidic linkages were observed in the cellulose nanoparticles, which are characteristic of the cellulose structure, also disappeared in the NMEAs samples.

However, no new peaks were observed as a result of incorporating the carbon-based materials with epoxy except in the case of the sample CNF-1.0, as the presence of the carboxyl groups on CNF was confirmed by the appearance of the stretching vibration of C═O at 1710 cm^{-1}, which suggested the formation of amides as a result of the reaction between C═O in CNF with amine in the epoxy hardener. It's noteworthy that FTIR studies showed no indication of chemical interaction between CNF and epoxy matrix, concluding that the immobilization of epoxy monomer on CNF is purely by physical interaction, as confirmed in Ref. [50].

For the silicon-based NMEAs samples (i.e. silica and clay samples), no any change (i.e. appearance and/or disappearance) of the chemical bonds took place in silica samples. While in the case of the clay samples, some functional groups disappeared from both epoxy and nanoparticle. For example, in agreement with [31,54,56–58], some of the peaks showed in the clay nanoparticles such as –OH stretching at 3627 cm^{-1}, –OH stretching, hydration at 3445 cm^{-1}, OH bending, hydration at 1636 cm^{-1}, can be attributed to adsorbed water molecules, and Al–Al–OH bending at 914 cm^{-1} or it is related to Si–O bond and Al–Fe–OH bending at 848 cm^{-1}. All those peaks disappeared in the clay NMEAs. In addition, the peak that was observed at 3305 cm^{-1} for N–H bending vibration/N–H stretching in the neat epoxy disappeared in the clay NMEAs samples.

3.4. Raman spectroscopy

As presented in the introduction of this paper, one of the main indicators of the defects present on the structures of the carbon-based materials and those of their nanocomposites is the characteristics of the D- and G-bands and the corresponding I_D/I_G values.

The section introduces Raman spectroscopy as a technique to study defects in carbon-based materials and nanocomposites. It highlights the significance of the D- and G-bands and the I_D/I_G values in assessing structural defects. Raman spectra of the pristine carbon-based nanomaterials (CNF and graphite) and their respective nanocomposites (CNF NMEAs and graphite NMEAs) are presented and discussed. The location of D and G bands, their intensities, and the I_D/I_G values are provided for each sample. These parameters offer insights into the quality and defects of the carbon-based nanomaterials and the resulting nanocomposites.

The results of Raman analysis of the NE, CNF and graphite NMEAs are included in this section. Raman spectra of tested samples are shown in Fig. 6 and the locations of both D and G-bands, their corresponding intensities in addition to the I_D/I_G values of the pristine CNF and graphite and their NMEAs are listed in Table 6.

As shown in Table 6, the D-band values of the CNF NMEAs samples followed the order 0.5 > 1.0>1.5, which agrees with that of the crystallinity values of those samples. This was attributed to that the D peak associated with nano-crystalline carbon. The same observation was found in the graphene NMEAs samples. Moreover, the higher D peak means that the sp^2 bonds are broken which in turn means that there are more sp^3 bonds and more transition from sp^2 to sp^3 material, as the nanoparticles concentration increases. In addition, since G-band arises from the stretching of the C–C bond in graphitic materials, it was noticed that the order (i.e. 0.5 < 1.0<1.5) of the G-band of the CNF and graphite

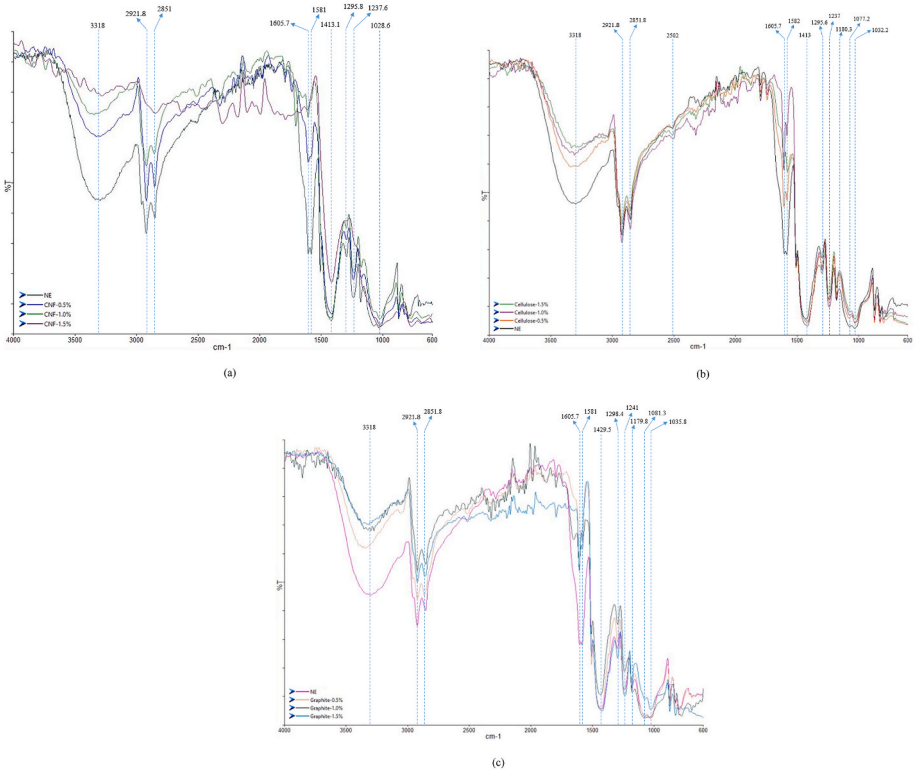

Fig. 5. FTIR spectrum showing the differences in the intensity orders of the functional groups of (a) NE and CNF nanocomposites, (b) NE and cellulose nanocomposites and (c) NE and graphite nanocomposites.

NMEAs samples agreed with what was found in the FTIR analysis in regard with the intensity order of C–C stretching at 1581 cm^{-1} and 1605.7 (only in CNF). Moreover, it was also observed that the G-peak, as shown in Fig. 6, did split into two peaks in some of the NMEAs, e.g. G-peak (1575-1585 cm^{-1}) and D′-peak (~1610-1620 cm^{-1}), which was ascribed to the presence of some randomly distributed impurities or surface charges in the samples.

The I_D/I_G of the carbon-based nanocomposites were higher than those of the pristine materials, which means that incorporating the nanoparticle into epoxy adhesive led the structure of the nanomaterial to defect which results in decreasing in ordering of sp^2 bonded graphitic domains. Moreover, the order of the I_D/I_G of the graphite nanocomposites, which was in agreement with that of the intensity of C–O–C str. at 1035.8 cm^{-1}, confirmed that the oxidation of carbon material leads to that sp^2 bonds to break which in turn means that there are more sp^3 bonds and more transition from sp^2 to sp^3 material, which would eventually lead to higher I_D/I_G, as it is directly related to sp^3/sp^2 carbon ratio. These observations are in contradict with what was found by Zhao et al. [3], as it was observed that incorporating epoxy had no effect on the I_D/I_G in the spectra of the pristine material (i.e. SWCNTs).

It's noteworthy that the presence of the D and G bands in the NMEAs in those ranges, as shown in Table 6, that belong to carbon-based materials indicated a good dispersion of the nanoparticles in epoxy, as confirmed in the literature [1,42].

4. Conclusions

In this study, multiple nanomaterial-modified epoxy adhesives (NMEAs) were prepared by incorporating carbon- and silicon-based nanomaterials into neat structural epoxy (NE) adhesive at concentrations of 0.5, 1.0 and 1.5 wt%. Various characterizations of the NE and NMEAs were conducted using SEM, XRD (i.e. crystallinity), FTIR, and Raman spectroscopies to investigate their microstructural characteristics, physical state and chemical composition, respectively. The results obtained from different analyses were individually assessed and were also correlated for a comprehensive assessment, leading to the following conclusions.

1. Using such simple and cost-effective synthesis method (i.e. a combination of manual mixing and ultra-sonication) resulted in producing nanocomposites with relatively good dispersion (but not agglomeration-free) of the nanoparticles within the epoxy matrix.
2. As the concentration of nanoparticles increased, their tendency to agglomerate also increased. These agglomerations tend to occupy certain areas within the material denser compared to other regions.
3. Irregularities introduced by the agglomerations, with both densely packed areas, collectively result in a higher level of porosity in the produced nanocomposites, which had higher % porosity as the nanoparticles' concentration increased. Furthermore, more % porosity increase was observed when going from 0.5 to 1.0 wt% concentrations compared to going from 1.0 to 1.5 wt%.
4. Porosity performance within the carbon-based nanocomposites exhibits concentration-dependent variations, with "CNF < cellulose < graphite" at concentrations ranging from 0.5 to 1.0 wt%, but shifting to "CNF < graphite < cellulose" at concentrations from 1.0 to 1.5 wt %. In contrast, silicon-based nanocomposites consistently maintain the order of % porosity increase (clay ≫ silica) across all concentration ranges. This distinction underscores the complexity of carbon-based systems, while silicon-based counterparts demonstrate a more consistent behaviour in porosity reduction.
5. Both nanoparticle agglomerations and increased % porosity contributed to the overall reduction in crystallinity in all nanocomposites compared to that of the NE. in addition, the nanocomposites became less crystalline much more when the concentration was doubled (from 0.5 to 1.0 wt%) than when it was just increased by half more (from 1.0 to 1.5 wt%).
6. According to the results obtained from FTIR spectroscopy, the intensities of chemical bonds in both NE and carbon-based

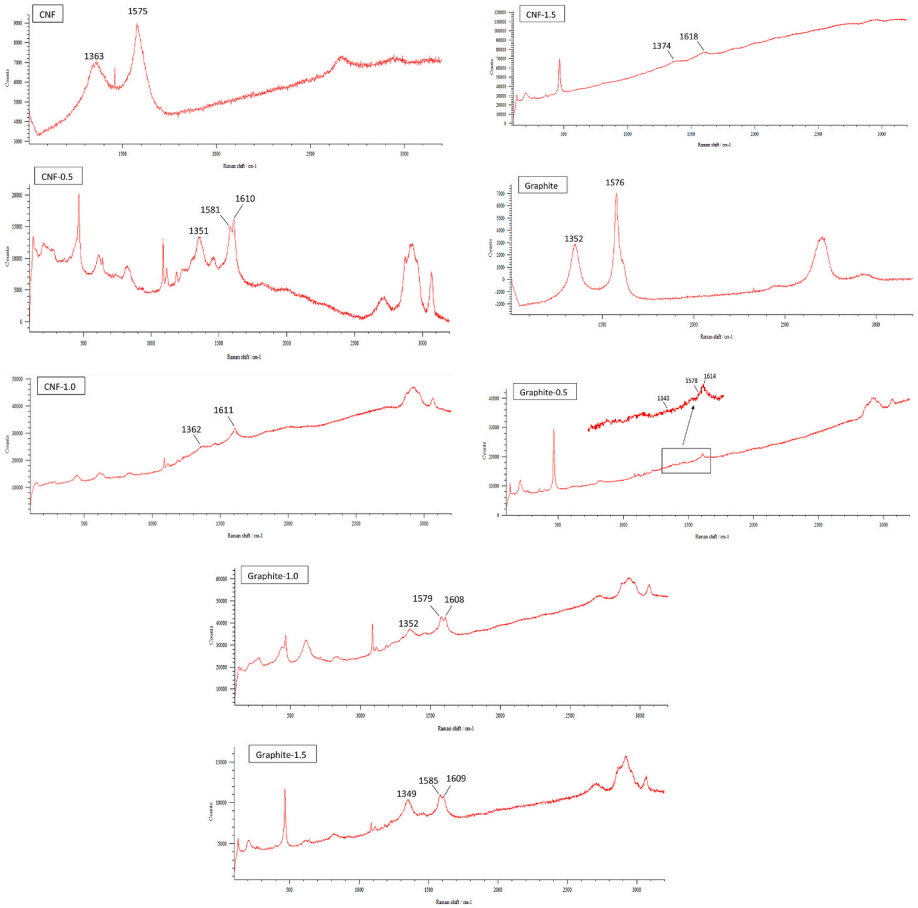

Fig. 6. Raman spectra of the pristine carbon-based nanomaterials and their NMEAs.

Table 6
Locations and intensities of the D- and G-bands and the corresponding I_D/I_G values of the pristine CNF and graphite and their NMEAs.

Sample	D-band (location (cm^{-1}) -intensity)	G- band (location (cm^{-1}) -intensity)	I_D/I_G
CNF (pristine material)	1363–7066.96	1575–8978.22	0.7871
CNF-0.5	1374–13538.5	1579–15136.2	0.8944
CNF-1.0	1362–25111.5	1611–31733.1	0.7913
CNF-1.5	1351–67322.5	1618–77236.1	0.8716
Graphite (pristine material)	1352–2924.27	1576–7051.46	0.4147
Graphite-0.5	1343–16811.4	1578–19550.3	0.8599
Graphite-1.0	1352–37270.4	1579–42802.2	0.8708
Graphite1.5	1349–10447.7	1585–11072.9	0.9435

nanocomposites were found to change based on the type of the nanomaterial and its concentration in the epoxy matrix.

7. No new chemical bonds were formed when carbon-based materials were incorporated, except for CNF-1.0, which showed the formation of a specific bond (C═O stretching at 1710 cm^{-1}). However, some functional groups disappeared in the nanocomposites. On the other hand, the silicon-based materials did not introduce any changes (neither appearance of disappearance) in the chemical bonds that already exist in the NE.
8. The Raman spectroscopy results revealed that both CNF and graphite NMEAs exhibited higher I_D/I_G values compared to their pristine materials. Furthermore, for CNF NMEAs, the D-band values followed the order 0.5 > 1.0 >1.5, whereas the G-band values showed the opposite order of 0.5 < 1.0 <1.5. A similar G-bands trend was observed in graphite NMEAs, with a D-band order of 0.5 < 1.5 <1.0.

Declaration of competing interest

The authors declare that they have no known competing financial interests or personal relationships that could have appeared to influence the work reported in this paper.

Data availability

Data will be made available on request.

References

[1] X. Wang, W. Xing, X. Feng, B. Yu, L. Song, Y. Hu, Functionalization of graphene with grafted polyphosphamide for flame retardant epoxy composites: synthesis, flammability and mechanism, Polym. Chem. 5 (4) (2014) 1145–1154.
[2] Y. Nie, T. Hübert, Effect of carbon nanofiber (CNF) silanization on the properties of CNF/epoxy nanocomposites, Polym. Int. 60 (11) (2011) 1574–1580.
[3] S. Zhao, Z. Song, J. Cui, C. Li, Y. Yan, Improving dispersion and integration of single-walled carbon nanotubes in epoxy composites by using a reactive noncovalent dispersant, J. Polym. Sci. Polym. Chem. 50 (21) (2012) 4548–4556.
[4] S. Gantayat, D. Rout, S.K. Swain, Carbon nanomaterial–reinforced epoxy composites: a review, Polym.-Plast. Technol. Eng. 57 (1) (2018) 1–16.
[5] M. Al-Zu'bi, M. Fan, L. Anguilano, Advances in bonding agents for retrofitting concrete structures with fibre reinforced polymer materials: a review, Construct. Build. Mater. 330 (2022), 127115.
[6] Y. Iwahori, S. Ishiwata, T. Sumizawa, T. Ishikawa, Mechanical properties improvements in two-phase and three-phase composites using carbon nano-fiber dispersed resin, Compos. Appl. Sci. Manuf. 36 (10) (2005) 1430–1439.
[7] Y. Zhou, F. Pervin, S. Jeelani, Effect vapor grown carbon nanofiber on thermal and mechanical properties of epoxy, J. Mater. Sci. 42 (17) (2007) 7544–7553.

[8] R. Al-Safy, R. Al-Mahaidi, G.P. Simon, Thermal and mechanical characterizations of nanomaterial-modified adhesive used in bonding CFRP to concrete, J. Adhes. 87 (7–8) (2011) 842–857.
[9] J. Zhu, S. Wei, J. Ryu, M. Budhathoki, G. Liang, Z. Guo, In situ stabilized carbon nanofiber (CNF) reinforced epoxy nanocomposites, J. Mater. Chem. 20 (23) (2010) 4937–4948.
[10] R.B. Ladani, S. Wu, A.J. Kinloch, K. Ghorbani, J. Zhang, A.P. Mouritz, C.H. Wang, Multifunctional properties of epoxy nanocomposites reinforced by aligned nanoscale carbon, Mater. Des. 94 (2016) 554–564.
[11] B.B. Johnsen, A.J. Kinloch, R.D. Mohammed, A.C. Taylor, S. Sprenger, Toughening mechanisms of nanoparticle-modified epoxy polymers, Polymer 48 (2) (2007) 530–541.
[12] Y.L. Liu, W.L. Wei, K.Y. Hsu, W.H. Ho, Thermal stability of epoxy-silica hybrid materials by thermogravimetric analysis, Thermochim. Acta 412 (1–2) (2004) 139–147.
[13] N. Chisholm, H. Mahfuz, V.K. Rangari, A. Ashfaq, S. Jeelani, Fabrication and mechanical characterization of carbon/SiC-epoxy nanocomposites, Compos. Struct. 67 (1) (2005) 115–124.
[14] S.A. Morshed, T.J. Young, W.M. Chirdon, Q. Zhang, J. Tatar, Durability of wet lay-up FRP bonded to concrete with nanomodified epoxy adhesives, J. Adhes. (2018).
[15] M. Hosur, T.H. Mahdi, M.E. Islam, S. Jeelani, Mechanical and viscoelastic properties of epoxy nanocomposites reinforced with carbon nanotubes, nanoclay, and binary nanoparticles, J. Reinforc. Plast. Compos. 36 (9) (2017) 667–684.
[16] E. Huttunen-Saarivirta, G.V. Vaganov, V.E. Yudin, J. Vuorinen, Characterization and corrosion protection properties of epoxy powder coatings containing nanoclays, Prog. Org. Coating 76 (4) (2013) 757–767.
[17] P. Baruah, N. Karak, Bio-based tough hyperbranched epoxy/graphene oxide nanocomposite with enhanced biodegradability attribute, Polym. Degrad. Stabil. 129 (2016) 26–33.
[18] C. Bao, Y. Guo, L. Song, Y. Kan, X. Qian, Y. Hu, In situ preparation of functionalized graphene oxide/epoxy nanocomposites with effective reinforcements, J. Mater. Chem. 21 (35) (2011) 13290–13298.
[19] B.S. Tk, A.B. Nair, B.T. Abraham, P.S. Beegum, E.T. Thachil, Microwave exfoliated reduced graphene oxide epoxy nanocomposites for high performance applications, Polymer 55 (16) (2014) 3614–3627.
[20] A. Kumar, D.K. Chouhan, P.S. Alegaonkar, T.U. Patro, Graphene-like nanocarbon: an effective nanofiller for improving the mechanical and thermal properties of polymer at low weight fractions, Compos. Sci. Technol. 127 (2016) 79–87.
[21] S. Chandrasekaran, C. Seidel, K. Schulte, Preparation and characterization of graphite nano-platelet (GNP)/epoxy nano-composite: mechanical, electrical and thermal properties, Eur. Polym. J. 49 (12) (2013) 3878–3888.
[22] S. Park, D.S. Kim, Curing behavior and physical properties of an epoxy nanocomposite with amine-functionalized graphene nanoplatelets, Compos. Interfac. 23 (7) (2016) 675–687.
[23] L. Chen, P. Zhao, H. Xie, W. Yu, Thermal properties of epoxy resin based thermal interfacial materials by filling Ag nanoparticle-decorated graphene nanosheets, Compos. Sci. Technol. 125 (2016) 17–21.
[24] G. Bogoeva-Gaceva, E. Mäder, L. Häußler, K. Sahre, Parameters affecting the interface properties in carbon fibre/epoxy systems, Composites 26 (2) (1995) 103–107.
[25] J. Guo, Y. Li, S. Wu, W. Li, The effects of γ-irradiation dose on chemical modification of multi-walled carbon nanotubes, Nanotechnology 16 (10) (2005) 2385.
[26] P. Jojibabu, Y.X. Zhang, A.N. Rider, J. Wang, B.G. Prusty, Synergetic effects of carbon nanotubes and triblock copolymer on the lap shear strength of epoxy adhesive joints, Compos. B Eng. 178 (2019), 107457.
[27] S.K. Hong, D. Kim, S. Lee, B.W. Kim, P. Theilmann, S.H. Park, Enhanced thermal and mechanical properties of carbon nanotube composites through the use of functionalized CNT-reactive polymer linkages and three-roll milling, Compos. Appl. Sci. Manuf. 77 (2015) 142–146.
[28] S.N. Ahn, H.J. Lee, B.J. Kim, L.S. Tan, J.B. Baek, Epoxy/amine-functionalized short-length vapor-grown carbon nanofiber composites, J. Polym. Sci. Polym. Chem. 46 (22) (2008) 7473–7482.
[29] P.C. Ma, S.Y. Mo, B.Z. Tang, J.K. Kim, Dispersion, interfacial interaction and re-agglomeration of functionalized carbon nanotubes in epoxy composites, Carbon 48 (6) (2010) 1824–1834.
[30] T. Ramanathan, F.T. Fisher, R.S. Ruoff, L.C. Brinson, Amino-functionalized carbon nanotubes for binding to polymers and biological systems, Chem. Mater. 17 (6) (2005) 1290–1295.
[31] B. Tyagi, C.D. Chudasama, R.V. Jasra, Determination of structural modification in acid activated montmorillonite clay by FT-IR spectroscopy, Spectrochim. Acta Mol. Biomol. Spectrosc. 64 (2) (2006) 273–278.
[32] R. Wang, G. Jiang, Y. Ding, Y. Wang, X. Sun, X. Wang, W. Chen, Photocatalytic activity of heterostructures based on TiO2 and halloysite nanotubes, ACS Appl. Mater. Interfaces 3 (10) (2011) 4154–4158.
[33] X. Wang, F. Tang, Q. Cao, X. Qi, M. Pearson, M. Li, H. Pan, Z. Zhang, Z. Lin, Comparative study of three carbon additives: carbon nanotubes, graphene, and fullerene-c60, for synthesizing enhanced polymer nanocomposites, Nanomaterials 10 (5) (2020) 838.
[34] Z.H. Shengtao, G. Anyan, G. Huanfang, C.H. Xiangqian, Characterization of Exfoliated Graphite Prepared with the Method of Secondary Intervening, 2011.
[35] S. Andreev, D. Purgina, E. Bashkatova, A. Garshev, A. Maerle, I. Andreev, N. Osipova, N. Shershakova, M. Khaitov, Study of fullerene aqueous dispersion prepared by novel dialysis method: simple way to fullerene aqueous solution, Fullerenes, Nanotub. Carbon Nanostruct. 23 (9) (2015) 792–800.
[36] Y. Zhang, H. Chi, W. Zhang, Y. Sun, Q. Liang, Y. Gu, R. Jing, Highly efficient adsorption of copper ions by a PVP-reduced graphene oxide based on a new adsorption's mechanism, Nano-Micro Lett. 6 (1) (2014) 80–87.
[37] F. Pahlevanzadeh, R. Emadi, M. Setayeshmehr, M. Kharaziha, S.A. Poursamar, Antibacterial Amorphous Magnesium Phosphate/graphene Oxide for Accelerating Bone Regeneration, Biomaterials Advances, 2022, 212856.
[38] S. Kujur, D.D. Pathak, Reduced graphene oxide-immobilized iron nanoparticles Fe (0)@ rGO as heterogeneous catalyst for one-pot synthesis of series of propargylamines, Res. Chem. Intermed. 46 (1) (2020) 369–384.
[39] P. Galvez, S.L. de Armentia, J. Abenojar, M.A. Martinez, Effect of moisture and temperature on thermal and mechanical properties of structural polyurethane adhesive joints, Compos. Struct. 247 (2020), 112443.
[40] A. Allaoui, S. Bai, H.M. Cheng, J.B. Bai, Mechanical and electrical properties of a MWNT/epoxy composite, Compos. Sci. Technol. 62 (15) (2002) 1993–1998.
[41] T.C. Rousakis, K.B. Kouravelou, T.K. Karachalios, Effects of carbon nanotube enrichment of epoxy resins on hybrid FRP–FR confinement of concrete, Compos. B Eng. 57 (2014) 210–218.
[42] Z. Zhang, W. Zhang, D. Li, Y. Sun, Z. Wang, C. Hou, L. Chen, Y. Cao, Y. Liu, Mechanical and anticorrosive properties of graphene/epoxy resin composites coating prepared by in-situ method, Int. J. Mol. Sci. 16 (1) (2015) 2239–2251.
[43] M.M. Shokrieh, M. Esmkhani, Z. Shokrieh, Z. Zhao, Stiffness prediction of graphene nanoplatelet/epoxy nanocomposites by a combined molecular dynamic–micromechanics method, Comput. Mater. Sci. 92 (2014) 444–450.
[44] L.H. Sun, Z. Ounaies, X.L. Gao, C.A. Whalen, Z.G. Yang, Preparation, characterization, and modeling of carbon nanofiber/epoxy nanocomposites, J. Nanomater. (2011), 2011.
[45] A. Allaoui, S.V. Hoa, M.D. Pugh, The electronic transport properties and microstructure of carbon nanofiber/epoxy composites, Compos. Sci. Technol. 68 (2) (2008) 410–416.
[46] L. Thompson, M. Nikzad, I. Sbarski, A. Yu, Esterified cellulose nanocrystals for reinforced epoxy nanocomposites, Prog. Nat. Sci.: Mater. Int. (2022).
[47] E. Abraham, D. Kam, Y. Nevo, R. Slattegard, A. Rivkin, S. Lapidot, O. Shoseyov, Highly modified cellulose nanocrystals and formation of epoxy-nanocrystalline cellulose (CNC) nanocomposites, ACS Appl. Mater. Interfaces 8 (41) (2016) 28086–28095.
[48] T. Aziz, H. Fan, X. Zhang, F.U. Khan, S. Fahad, A. Ullah, Adhesive properties of bio-based epoxy resin reinforced by cellulose nanocrystal additives, J. Polym. Eng. 40 (4) (2020) 314–320.
[49] S.X. Peng, S. Shrestha, Y. Yoo, J.P. Youngblood, Enhanced dispersion and properties of a two-component epoxy nanocomposite using surface modified cellulose nanocrystals, Polymer 112 (2017) 359–368.
[50] A. Tanvir, Y.H. El-Gawady, M. Al-Maadeed, Cellulose nanofibers to assist the release of healing agents in epoxy coatings, Prog. Org. Coating 112 (2017) 127–132.
[51] L. Yue, A. Maiorana, F. Khelifa, A. Patel, J.M. Raquez, L. Bonnaud, R. Gross, P. Dubois, I. Manas-Zloczower, Surface-modified cellulose nanocrystals for biobased epoxy nanocomposites, Polymer 134 (2018) 155–162.
[52] T. Aziz, H. Fan, X. Zhang, F.U. Khan, S. Fahad, A. Ullah, Adhesive properties of bio-based epoxy resin reinforced by cellulose nanocrystal additives, J. Polym. Eng. 40 (4) (2020) 314–320.
[53] Z. Sun, Y. Liu, R. Wong, M. Yu, J. Li, M. Moran, M. Kathaperumal, C.P. Wong, Crumpled Graphene Epoxy Nanocomposites Modified with Polydopamine for Advanced Semiconductor Packaging Applications, Composites Science and Technology, 2022, 109709.
[54] O. Zabihi, H. Khayyam, B.L. Fox, M. Naebe, Enhanced thermal stability and lifetime of epoxy nanocomposites using covalently functionalized clay: experimental and modelling, New J. Chem. 39 (3) (2015) 2269–2278.
[55] D.E. Kherroub, M. Belbachir, S. Lamouri, L. Bouhadjar, K. Chikh, Synthesis of polyamide-6/montmorillonite nanocomposites by direct in-situ polymerization catalysed by exchanged clay, Orient. J. Chem. 29 (4) (2013) 1429.
[56] K. Xu, K. Li, D. Tu, T. Zhong, C. Xie, Reinforcement on the mechanical-, thermal-, and water-resistance properties of the wood flour/chitosan/poly (vinyl chloride) composites by physical and chemical modification, J. Appl. Polym. Sci. 131 (18) (2014).
[57] K. Majdzadeh-Ardakani, S. Zekriardehani, M.R. Coleman, S.A. Jabarin, A novel approach to improve the barrier properties of PET/clay nanocomposites, Int. J. Polym. Sci. (2017), 2017.
[58] S. Thomas, D. Rouxel, D. Ponnamma (Eds.), Spectroscopy of Polymer Nanocomposites, William Andrew, 2016.
[59] N. Mahmood, M. Islam, A. Hameed, S. Saeed, Polyamide 6/multiwalled carbon nanotubes nanocomposites with modified morphology and thermal properties, Polymers 5 (4) (2013) 1380–1391.
[60] Morimune, S., Nishino, T. and Goto, T., Graphene Oxide Reinforced Poly (Vinyl Alcohol) Nanocomposites..
[61] A. Bhattacharyya, S. Chen, M. Zhu, Graphene reinforced ultra-high molecular weight polyethylene with improved tensile strength and creep resistance properties, Express Polym. Lett. 8 (2) (2014).
[62] E. Werner, Zyl van, M. Garcia, B.A.G. Schrauwen, B.J. Kooi, J.Th M. De Hosson, Hybrid polyamide/silica nanocomposites: synthesis and mechanical testing, Macromol. Mater. Eng. 287 (2002) 106.
[63] M. Sadeghi, G. Khanbabaei, A.H.S. Dehaghani, M. Sadeghi, M.A. Aravand, M. Akbarzade, S. Khatti, Gas permeation properties of ethylene vinyl acetate–silica nanocomposite membranes, J. Membr. Sci. 322 (2) (2008) 423–428.

[64] L. Chen, K. Zheng, X. Tian, K. Hu, R. Wang, C. Liu, Y. Li, P. Cui, Double glass transitions and interfacial immobilized layer in in-situ-synthesized poly (vinyl alcohol)/silica nanocomposites, Macromolecules 43 (2) (2010) 1076–1082.
[65] Z. Peng, L.X. Kong, S.D. Li, P. Spiridonov, Poly (vinyl alcohol)/silica nanocomposites: morphology and thermal degradation kinetics, J. Nanosci. Nanotechnol. 6 (12) (2006) 3934–3938.
[66] A. Kumar, Y. S Negi, N. K Bhardwaj, V. Choudhary, Synthesis and characterization of cellulose nanocrystals/PVA based bionanocomposite, Advanced materials letters 4 (8) (2013) 626–631.
[67] M.A. Alam, U.A. Samad, A. Anis, M. Alam, M. Ubaidullah, S.M. Al-Zahrani, Effects of SiO2 and ZnO nanoparticles on epoxy coatings and its performance investigation using thermal and nanoindentation technique, Polymers 13 (9) (2021) 1490.
[68] U. Marathe, A. Chalana, J. Bijwe, Performance augmentation of epoxy adhesives with TiN nanoparticles, ACS Omega 7 (5) (2022) 4150–4157.
[69] P. Jojibabu, M. Jagannatham, P. Haridoss, G.J. Ram, A.P. Deshpande, S.R. Bakshi, Effect of different carbon nano-fillers on rheological properties and lap shear strength of epoxy adhesive joints, Compos. Appl. Sci. Manuf. 82 (2016) 53–64.
[70] K.S. Kim, K.Y. Rhee, K.H. Lee, J.H. Byun, S.J. Park, Rheological behaviors and mechanical properties of graphite nanoplate/carbon nanotube-filled epoxy nanocomposites, J. Ind. Eng. Chem. 16 (4) (2010) 572–576.
[71] S.A. Sydlik, J.H. Lee, J.J. Walish, E.L. Thomas, T.M. Swager, Epoxy functionalized multi-walled carbon nanotubes for improved adhesives, Carbon 59 (2013) 109–120.
[72] Z. Fan, S.G. Advani, Rheology of multiwall carbon nanotube suspensions, J. Rheol. 51 (4) (2007) 585–604.
[73] J.A. Kim, D.G. Seong, T.J. Kang, J.R. Youn, Effects of surface modification on rheological and mechanical properties of CNT/epoxy composites, Carbon 44 (10) (2006) 1898–1905.
[74] A.C. Ackermann, S. Carosella, M. Rettenmayr, B.L. Fox, P. Middendorf, Rheology, dispersion, and cure kinetics of epoxy filled with amine-and non-functionalized reduced graphene oxide for composite manufacturing, J. Appl. Polym. Sci. 139 (8) (2022), 51664.
[75] A. Montazeri, The effect of functionalization on the viscoelastic behavior of multi-wall carbon nanotube/epoxy composites, Mater. Des. 45 (2013) 510–517.
[76] H. Miyagawa, L.T. Drzal, Thermo-physical and impact properties of epoxy nanocomposites reinforced by single-wall carbon nanotubes, Polymer 45 (15) (2004) 5163–5170.
[77] Y. Zhao, E.V. Barrera, Asymmmetric diamino functionalization of nanotubes assisted by BOC protection and their epoxy nanocomposites, Adv. Funct. Mater. 20 (18) (2010) 3039–3044.
[78] Y. Zhou, F. Pervin, L. Lewis, S. Jeelani, Fabrication and characterization of carbon/epoxy composites mixed with multi-walled carbon nanotubes, Mater. Sci. Eng., A 475 (1–2) (2008) 157–165.
[79] F.L. Jin, S.J. Park, Thermal properties of epoxy resin/filler hybrid composites, Polym. Degrad. Stabil. 97 (11) (2012) 2148–2153.
[80] F.H. Gojny, M.H. Wichmann, B. Fiedler, K. Schulte, Influence of different carbon nanotubes on the mechanical properties of epoxy matrix composites–a comparative study, Compos. Sci. Technol. 65 (15–16) (2005) 2300–2313.
[81] C. Wang, H. Ge, H. Liu, S. Guo, Microstructure and properties of carbon fiber sized with pickering emulsion based on graphene oxide sheets and its composite with epoxy resin, J. Appl. Polym. Sci. 132 (29) (2015).
[82] R. Moriche, S.G. Prolongo, M. Sánchez, A. Jiménez-Suárez, F.J. Chamizo, A. Ureña, Thermal conductivity and lap shear strength of GNP/epoxy nanocomposites adhesives, Int. J. Adhesion Adhes. 68 (2016) 407–410.
[83] P. Jongvivatsakul, C. Thongchom, A. Mathuros, T. Prasertsri, M. Adamu, S. Orasutthikul, A. Lenwari, T. Charainpanitkul, Enhancing bonding behavior between carbon fiber-reinforced polymer plates and concrete using carbon nanotube reinforced epoxy composites, Case Stud. Constr. Mater. 17 (2022), e01407.
[84] J.S. Tomblin, C. Yang, P. Harter, Investigation of Thick Bondline Adhesive Joints, WICHITA STATE UNIV KS, 2001.
[85] T. Filleter, R. Bernal, S. Li, H.D. Espinosa, Ultrahigh strength and stiffness in cross-linked hierarchical carbon nanotube bundles, Adv. Mater. 23 (25) (2011) 2855–2860.
[86] M. Mansourian-Tabaei, S.H. Jafari, H.A. Khonakdar, Lap shear strength and thermal stability of diglycidyl ether of bisphenol a/epoxy novolac adhesives with nanoreinforcing fillers, J. Appl. Polym. Sci. 131 (6) (2014).
[87] A. Wolf, A. Buchman, A. Eitan, T. Fine, Y. Nevo, A. Heyman, O. Shoseyov, Improved adhesives containing CNT/SP1 nano fillers, J. Adhes. 88 (4–6) (2012) 435–451.
[88] S. Gantayat, N. Sarkar, G. Prusty, D. Rout, S.K. Swain, Designing of epoxy matrix by chemically modified multiwalled carbon nanotubes, Adv. Polym. Technol. 37 (1) (2018) 176–184.
[89] M.L. Sham, J.K. Kim, Surface functionalities of multi-wall carbon nanotubes after UV/Ozone and TETA treatments, Carbon 44 (4) (2006) 768–777.
[90] P.C. Ma, J.K. Kim, B.Z. Tang, Effects of silane functionalization on the properties of carbon nanotube/epoxy nanocomposites, Compos. Sci. Technol. 67 (14) (2007) 2965–2972.
[91] Y.K. Choi, K.I. Sugimoto, S.M. Song, Y. Gotoh, Y. Ohkoshi, M. Endo, Mechanical and physical properties of epoxy composites reinforced by vapor grown carbon nanofibers, Carbon 43 (10) (2005) 2199–2208.
[92] A.C. Ackermann, M. Fischer, A. Wick, S. Carosella, B.L. Fox, P. Middendorf, Mechanical, thermal and electrical properties of epoxy nanocomposites with amine-functionalized reduced graphene oxide via plasma treatment, J. Composit. Sci. 6 (6) (2022) 153.
[93] M.G. Kim, J.B. Moon, C.G. Kim, Effect of CNT functionalization on crack resistance of a carbon/epoxy composite at a cryogenic temperature, Compos. Appl. Sci. Manuf. 43 (9) (2012) 1620–1627.
[94] W. Liu, S.V. Hoa, M. Pugh, Organoclay-modified high performance epoxy nanocomposites, Compos. Sci. Technol. 65 (2) (2005) 307–316.
[95] S. Gantayat, G. Prusty, D.R. Rout, S.K. Swain, Expanded graphite as a filler for epoxy matrix composites to improve their thermal, mechanical and electrical properties, N. Carbon Mater. 30 (5) (2015) 432–437.
[96] N.A. Siddiqui, R.S. Woo, J.K. Kim, C.C. Leung, A. Munir, Mode I interlaminar fracture behavior and mechanical properties of CFRPs with nanoclay-filled epoxy matrix, Compos. Appl. Sci. Manuf. 38 (2) (2007) 449–460.
[97] J. Michels, J.S. Cruz, R. Christen, C. Czaderski, M. Motavalli, Mechanical performance of cold-curing epoxy adhesives after different mixing and curing procedures, Compos. B Eng. 98 (2016) 434–443.
[98] F. Lapique, K. Redford, Curing effects on viscosity and mechanical properties of a commercial epoxy resin adhesive, Int. J. Adhesion Adhes. 22 (4) (2002) 337–346.
[99] B. Bilyeu, W. Brostow, K.P. Menard, Epoxy thermosets and their applications I: chemical structures and applications, J. Mater. Educ. 21 (5/6) (1999) 281–286.
[100] B. Bilyeu, W. Brostow, K.P. Menard, Epoxy thermosets and their applications II. Thermal analysis, J. Mater. Educ. 22 (4/6) (2000) 107–130.
[101] B. Bilyeu, W. Brostow, K.P. Menard, Epoxy thermosets and their applications. III. Kinetic equations and models, J. Mater. Educ. 23 (4–6) (2001) 189–204.
[102] W. Brostow, H.E.H. Lobland, Materials: Introduction and Applications, John Wiley & Sons, 2016.